Macromolecules
ARTICLE

Macromolecules **2010**, *43*, 2463–2473 **2463**
DOI: 10.1021/ma901693c

Composition-Dependent Morphological Transitions and Pathways in Switching of Fine Structure in Thin Films of Block Copolymer Supramolecular Assemblies

Bhanu Nandan,* Mukesh Kumar Vyas,† Marcus Böhme, and Manfred Stamm*

Leibniz Institute of Polymer Research Dresden, Hohe Strasse 6, 01069 Dresden, Germany. †Present address: Institute of Polymer Research, GKSS Research Centre Geesthacht GmbH, 21502 Geesthacht, Germany.

Received July 30, 2009; Revised Manuscript Received February 4, 2010

ABSTRACT: The phase behavior of supramolecular assemblies (SMA) formed by polystyrene-*block*-poly(4-vinylpyridine) (PS-*b*-P4VP) with 2-(4′-hydroxybenzeneazo)benzoic acid (HABA) was investigated with respect to the molar ratio (X) between HABA and 4VP monomer unit in bulk as well as in thin films coated on a silicon substrate. In bulk, the SMA showed bcc packed spherical or hexagonally packed cylindrical microdomains composed of P4VP(HABA) blocks in PS matrix depending on the composition which varied with the HABA weight fraction. However, at a molar ratio of 2 where HABA was in excess, the cylindrical microdomains of P4VP(HABA) blocks were found to pack in a tetragonal lattice. The SMA in thin film also showed spherical or cylindrical morphology depending on the composition. Interestingly, the orientation of cylindrical microdomains of P4VP(HABA) depended on the selectivity of the solvent as well as on the degree of swelling. Hence, in a nonselective solvent like chloroform, the cylinders were found to lie parallel to the substrate as long as the swelling ratio allowed the system to be in the cylindrical region of the phase diagram. At higher degree of swelling the cylinders transform into spherical domains, and drying of the solvent resulted in perpendicular orientation. In a selective solvent like 1,4-dioxane, the cylinders were found to be always oriented perpendicular to the substrate for $0.5 < X < 1.5$. Such a morphology was favored in this case, since even at a small degree of swelling, the system went into spherical morphology which ultimately resulted in perpendicular cylinders. The transformation from perpendicular to parallel domain orientation in chloroform, investigated using the ex-situ atomic force microscopy approach, involved domain breakup, induced by thermodynamically unstable interface, and then coalescence of the domains along the plane of the film. Moreover, at excess HABA concentration, a hexagonally perforated lamellar morphology was observed when the system was shortly exposed to chloroform vapors.

Introduction

Self-assembly is an incredibly powerful concept in modern molecular science. The ability of carefully designed building blocks to spontaneously assemble into complex nanostructures underpins development in a wide range of technologies—ranging from materials science through to molecular biology.[1,2] Recently, self-assemblies of block copolymer-based systems have attracted considerable attention in the area of nanotechnology which relies largely on the ability to arrange functional domains at the nanoscale.[3−6] Block copolymers consisting of chemically different polymer chains form periodic nanostructures driven by the repulsive interaction between the constituent blocks. The phase behavior of linear diblock copolymers in bulk is now well-known. Since most of the applications of block copolymers rely on their structure formation at surfaces, hence, the self-assembly of block copolymers in thin films is being widely investigated.[3,4] The microphase separation of block copolymers in thin films, however, significantly differs from that in the bulk since the domain structure depends both on the surface energies and geometrical constraints. The interfacial energy plays a crucial role in orientation and ordering of microdomains in thin block copolymer films. In general, the preferential wetting of the substrate with one of the phases drives the system to the parallel alignment of nanodomains. In addition, the lowest surface tension component occupies the free surface of polymer film, enhancing the trend toward parallel alignment. The control on the orientation of cylindrical and parallel microdomains in block copolymer thin films is crucial and has received significant attention.[3,4]

Recently, it has been demonstrated that a strategy combining block copolymer self-assembly with supramolecular chemistry may provide a simple and powerful approach for controlling the formation of well-defined nanostructures.[10,11] It involves the selective functionalization of one of the blocks of the block copolymer by a low molecular additive through noncovalent interactions. Such supramolecular assemblies (SMA) have been investigated extensively in the past in bulk by Ikkala et al.[10−12] There are several advantages of the supramolecular approach in block copolymers. One is that by simply varying the low molecular weight additive fraction in the SMA, the morphology can be tailored. Another major advantage is that the low molecular weight additive can be selectively removed from the SMA by dissolution in a suitable solvent leading to nano-objects or nanoporous material where the original ordered morphology is retained. Significantly, the walls of the nano-objects or nanopores in such cases are lined with functional groups which provide interesting opportunities for nanotechnological applications.[12,13]

Though SMAs based on block copolymers have been extensively investigated in the bulk, their behavior in thin films is still to be fully understood. Moeller et al.[14] investigated the thin film morphologies of wedge-shaped liquid crystalline amphiphilic molecules complexed with poly(2-vinylpyridine)-*block*-poly(ethylene

*To whom correspondence should be addressed. E-mail: nandan@ipfdd.de (B.N.), stamm@ipfdd.de (M.S.).

© 2010 American Chemical Society

Published on Web 02/15/2010

oxide) (P2VP-*b*-PEO) diblock copolymer via proton transfer. The small molecules in this case were liquid crystalline, and their assembly dominated the assembly of the supramolecules. Recently, the thin films of supramolecular assemblies formed by PS-*b*-P4VP and pentadecylphenol (PDP) was investigated by ten Brinke et al.[15,16] The PDP was bound to pyridine group of 4VP unit via hydrogen bonding. They examined the phase behavior and terrace formation in this system after annealing it under different chloroform vapor pressures. It was observed that the P4VP(PDP) was present at the SiO_2 interface as well as at the air interface, implying symmetric boundary conditions, and the morphologies depended on the chloroform vapor pressure as well as on the formation of terraces. Xu et al.[17,18] investigated the hierarchical structures in thin films of PS-*b*-P4VP(PDP) supramolecular assembly. They found that the lamellar and cylindrical microdomains, with a periodicity of 40 nm, could be oriented normal to the surface, whereas the assembly of comb blocks, P4VP(PDP), with a periodicity of 4 nm, were oriented parallel to the surface. Furthermore, it was also shown that SMA approach may lead to certain nonequilibrium nanostructures different from its equilibrium morphology.[18]

In the above-mentioned studies on PS-*b*-P4VP(PDP) assemblies, the P4VP(PDP) either was the matrix phase or formed one of the layers of lamellar structures. However, for nanotechnological applications it is important that the low molecular additive is present either in the cylindrical microdomains, which preferably should be oriented perpendicular to the substrate, or in spherical microdomains. This is because, in these structures, the removal of low molecular weight additive will lead to nanopores which could then be used for nanopatterning applications. Nevertheless, it is possible to form cylindrical microdomains of P4VP(PDP) block by adjusting either the composition of the PS-*b*-P4VP block copolymer or by varying the PDP weight fraction in the SMA. However, our studies have shown that the obvious shortcoming in this case is that PDP being a surfactant preferably migrates to the surface, and hence the vertically oriented cylindrical microdomains of P4VP(PDP) block does not go through the complete film.[19]

Recently, our group reported the synthesis of SMA from PS-*b*-P4VP and 2-(4′-hydroxybenzeneazo)benzoic acid (HABA) where HABA selectively associated with the pyridine nitrogen via hydrogen bonding (Scheme 1).[20−24] Thin films of SMA demonstrated well-ordered hexagonal cylindrical morphology. The cylindrical nanodomains were formed by the P4VP(HABA) blocks surrounded by PS matrix. Significantly, the orientation of the cylindrical microdomains with respect to the film surface plane was found to depend on the solvent used for preparing the SMA. Hence, whereas the SMA film casted from 1,4-dioxane showed perpendicular cylinders, the film casted from chloroform showed parallel cylinders. Moreover, the orientation switched reversibly on exposing the SMA film to corresponding solvent. However, the mechanism of the switching phenomena was still unclear at that stage. Moreover, our previous study was limited to the SMA composition corresponding to stoichiometric ratio of 4VP units and HABA.

In the present paper, we investigate the microphase separation of PS-*b*-P4VP(HABA) SMA in bulk as well as in thin films in a wide range of compositions tuned by varying the molar ratio between HABA and 4VP unit. The nonstoichiometric compositions corresponded to deficient as well as excess HABA concentration relative to 4VP unit of P4VP block. It will be shown that the switching in the orientation of cylindrical microdomains persisted in a large composition window as long as the cylindrical morphology existed in the SMA. At low molar ratio, a morphological transition to spherical domains was observed, whereas at higher molar ratio, the microphase separation was much more complex. Furthermore, the solvent-induced orientational switching of cylindrical microdomains was also investigated, and a plausible mechanism for the structural reorganization during this switching will be presented.

Scheme 1

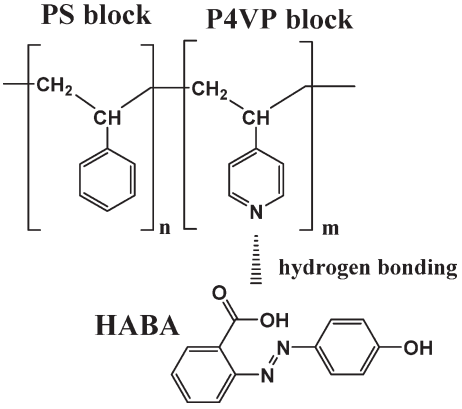

Table 1. Characteristics of PS-*b*-P4VP(HABA) SMA at Different HABA/4VP Molar Ratios

system	HABA/4VP (X)	$f_{P4VP(HABA)}$	f_{HABA}	bulk morphology
SMA0	0	0.091	0	bcc sphere
SMA025	0.25	0.132	0.048	bcc sphere
SMA050	0.50	0.172	0.092	hcp cylinder
SMA075	0.75	0.209	0.132	hcp cylinder
SMA100	1.00	0.242	0.168	hcp cylinder
SMA150	1.50	0.301	0.234	hcp cylinder
SMA200	2.00	0.352	0.289	sc cylinder

Experimental Section

Materials. Polystyrene-*block*-poly(4-vinylpyridine) (PS-*b*-P4VP), with number-averaged molecular masses (M_n) PS 35 500 g mol^{-1}, P4VP 3680 g mol^{-1}, and M_w/M_n = 1.06 for both blocks, was purchased from Polymer Source, Inc. 2-(4′-Hydroxybenzeneazo)benzoic acid (HABA) was purchased from Sigma-Aldrich. Solvents 1,4-dioxane, chloroform, and methanol were purchased from Acros Organics and used as is. Highly polished single-crystal silicon wafers of {100} orientation were purchased from Semiconductor Processing Co. and used as substrates. The silicon wafers were cleaned with dichloromethane in an ultrasonic bath for 20 min and then further in a 1:1:1 mixture of 29% ammonium hydroxide, 30% hydrogen peroxide, and water (*warning: this solution is extremely corrosive and should not be stored in tightly sealed containers*) for 1.5 h at 65 °C, finally rinsed several times with water, and dried in an argon flow.

Preparation of Supramolecular Assemblies. PS-*b*-P4VP-(HABA)$_X$ supramolecular assemblies were prepared in either chloroform or 1,4-dioxane, where X denotes the molar ratio given by the average number of HABA molecules bound to one monomer unit of P4VP block. The preweighed PS-*b*-P4VP and HABA were dissolved separately in the solvent. PS-*b*-P4VP solution was then slowly added dropwise to HABA solution while heating close to the boiling point of the solvent in an ultrasonic bath. The elevated temperature during mixing was very important for reproducible formation of SMA. The resulting 1 wt % solution was kept at least overnight to complete hydrogen-bond formation. Thin films were prepared by dip coating from the filtered (200 nm pore size PTFE filter) solutions. Detailed characteristics of the SMA investigated here are shown in Table 1. Bulk samples were prepared by slowly evaporating the solvent in a Petri dish over 2 weeks.

Solvent Vapor Treatment. The SMA thin films were further annealed in vapors of appropriate solvent for the reorientation of the microdomains and for improving the long-range order.

The solvent vapor treatment of the thin films were done in a crystallographic dish with a Petri dish containing the solvent. The silicon substrate coated with the SMA film was kept in this crystallographic dish which then was completely closed. The sample was removed from the dish after a predetermined time during which the solvent in the film quickly evaporated. The annealing time was recorded from the moment when samples were put into or taken out from the crystallographic dish. All the samples used in this study were solvent vapor treated in the same crystallographic dish for the comparative experiments.

Ellipsometry. The thickness of the polymer film was measured by a SE400 ellipsometer (SENTECH Instruments GmbH, Germany) with a 632.8 nm laser at a 70° incident angle. The thickness of all the samples coated on silicon substrate was kept constant at 40 ± 2 nm.

Small-Angle X-ray Scattering. SAXS measurements were performed in transmission geometry using a three-pinhole collimation system equipped with an Osmic multilayer mirror for higher photon flux at smaller beam spot and a Rigaku rotating anode generator (Cu Kα radiation $\lambda = 0.1542$ nm, operating at 4.2 kW with microfilament). For data collection, a Marccd detector with an average pixel size of 78.7 × 78.7 μm^2 was used. All scattering patterns were radially averaged to obtained the intensity $I(q)$, where $q = 4\pi/\lambda(\sin\theta/2)$. The data were corrected for background scattering, X-ray absorption, and thermal diffuse scattering.

Atomic Force Microscopy. Atomic force microscopy (AFM) imaging was performed using a Dimension 3100 scanning force microscope (Digital Instruments, Inc., Santa Barbara, CA) and a CP microscope (Park Scientific Instrument, Inc.) in the tapping mode. The tip characteristics were spring constant 1.5−3.7 N m^{-1}, resonant frequency 45−65 Hz, and tip radius about 10 nm. Analysis of the AFM images (fast Fourier transform and power spectral density) was performed with the WSxM software (Nanotec Electronica).

Transmission Electron Microscopy. The real-space morphology of the SMA was observed by using a FEI CM 200 transmission electron microscope at an accelerating voltage of 200 kV. The SMA sample was embedded in an epoxy resin and cured overnight at 40 °C. The sample was subsequently microtomed to a thickness of about 60 nm using a Leica Reichert Ultracut S ultramicrotome and a Diatome diamond knife at room temperature. The microtomed sections were floated on water and subsequently placed on copper grids. To obtain contrast during TEM, the samples were stained with iodine for 2 h.

Results and Discussion

Microphase Separation in Bulk. First, we discuss the microphase separation of the supramolecular assemblies in bulk as studied using SAXS. Figure 1 shows the SAXS profiles of the PS-*b*-P4VP(HABA)$_X$ SMA with different HABA/4VP molar ratio (X). The SAXS profiles shown in Figure 1a were obtained from the as-casted samples prepared by slow evaporation of the solvent, i.e., 1,4-dioxane, whereas the SAXS profiles in Figure 1b were obtained after further thermal annealing the sample at 140 °C for 48 h. The SAXS profiles of the as-casted samples of all the SMA show a primary scattering maximum between 0.2 and 0.35 nm^{-1}. The peak position of the primary scattering maximum shifted to low-q region as the molar ratio increased from 0.25 to 1.00. However, further increase in the molar ratio does not lead to any further change in the peak position of the primary scattering maximum. From Table 1, it could be speculated, considering the classical phase diagram of diblock copolymers, that the SMA with molar ratio of 0.25 and 0.50 will form bcc packed P4VP(HABA) spherical microdomains, whereas the SMA with higher molar ratio will form hexagonally packed (hcp) P4VP(HABA) cylindrical

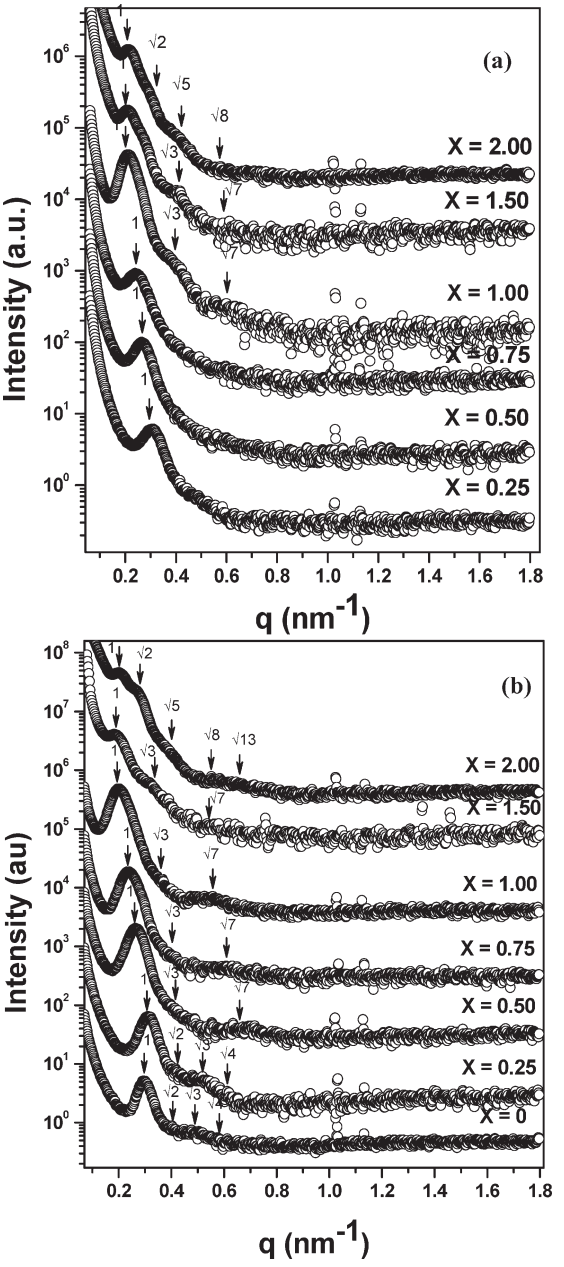

Figure 1. Room temperature SAXS intensity profiles of PS-*b*-P4VP(HABA) SMA for (a) as-casted samples and (b) annealed samples.

microdomains considering the volume fraction of the components. Here, it also must be noted that the phase diagram of the SMAs such as that studied in this work could be different than that of a simple diblock copolymer. The grafted structure of the P4VP(HABA) blocks will necessitate more interface space for the blocks and, hence, may shift the lamellar and cylindrical regions in the phase diagram toward lower volume fraction of P4VP(HABA). The higher order peaks in the SAXS profiles of as-casted samples were weak, and it was difficult to assign the morphology based on these profiles. However, for SMA100 and SMA150, a second-order peak could be clearly observed. The peak position of the two lattice peaks in the SAXS profiles were in the ratio $1:3^{1/2}$, indicating that the SMA100 and SMA150 contained hexagonally packed P4VP(HABA) cylinders in PS matrix. In the case of SMA200, the SAXS profile was much more complex. Apart from two clear lattice peaks in the ratio $1:3^{1/2}$, a faint and broad peak was also observed between

these two peaks whose position relative to the first-order peak ($2^{1/2}$) indicated tetragonally packed cylindrical morphology for this sample. As discussed below, for the annealed samples this issue was much more clear.

The thermal annealing of the SMA improved the ordering of the microdomains as is evidenced from the SAXS profiles obtained after annealing the samples (Figure 1b). The primary scattering peak was much more intense, and some of the higher order peaks could be clearly resolved. However, it must be noted here that, even after the annealing process, the bulk morphology of the SMAs were not highly ordered, and the absence or decreased intensity of few higher order peaks was due to small grain size of ordered domains and lattice distortion. This also broadened some of the higher order scattering peaks which led in some cases to overlapping of the nearby peaks. The SAXS profiles of neat PS-*b*-P4VP and SMA025 showed the lattice peaks in the ratio $1:2^{1/2}:3^{1/2}:4^{1/2}$, which indicated bcc packed spherical morphology as expected considering the volume fraction of the two blocks (Table 1). As could be noticed, the second-order peak in the SAXS profiles were very faint while the third- and fourth-order peaks overlapped. For SMA050, SMA075, and SMA100, the SAXS profile showed lattice peaks in the ratio $1:3^{1/2}:7^{1/2}$, which suggested hexagonally packed P4VP-(HABA) cylinders in these samples. For SMA150 also the lattice peaks in the SAXS profile were in the ratio $1:3^{1/2}:7^{1/2}$, and hence the cylinders were packed in a hexagonal lattice. However, the SAXS profile of SMA200 exhibited a different scattering pattern. The SAXS profile showed a primary scattering peak and several higher order lattice peaks which were in the ratio $1:2^{1/2}:4^{1/2}:5^{1/2}:8^{1/2}:13^{1/2}$ (also see Supporting Information). The broadening and overlapping of the higher order peaks ($4^{1/2}$,$5^{1/2}$ and $8^{1/2}$,$13^{1/2}$) could be noticed in this case also. These peaks are characteristic for scattering from a tetragonally packed lattice. Hence, in the case of SMA200, the P4VP(HABA) cylindrical microdomains, plausibly, were packed in a tetragonal lattice. The $2^{1/2}$, $4^{1/2}$, $5^{1/2}$, and $13^{1/2}$ peaks are associated with the (11), (20), (21), and (32) diffraction planes, respectively, of a square lattice organized by the P4VP(HABA) cylindrical microdomains. The tetragonal packing of the P4VP(HABA) cylinders was further confirmed by the real-space morphological observation by TEM. Figure 2 shows the TEM micrograph of the microtomed ultrathin sections stained by iodine. Since iodine is a preferential staining agent for P4VP, the P4VP(HABA) cylindrical domains appear dark in the image. The TEM micrograph clearly demonstrates the tetragonal organization of P4VP(HABA) cylinders in PS matrix as is also evident from the corresponding FFT patterns which shows 4-fold symmetry.

The cylindrical domains formed by diblock copolymers have been found to organize almost exclusively in a hexagonal lattice due to its efficiency for space filling. Tetragonal lattice is observed only when some special factors are introduced to modify the intermicellar interactions. Tetragonal lattice has been observed in the past in some liquid crystalline systems,[25] in ABC triblock copolymers,[26] and also in blends of diblock copolymer with supramolecular interactions.[27] Recently, Chen and co-workers[28,29] have shown the presence of tetragonally packed cylindrical microdomains in supramolecular comb−coil block copolymers. They showed that in supramolecular assemblies formed by PS-*b*-P4VP and an amphiphilic surfactant, dodecylbenzenesulfonic acid (DBSA), at stoichiometric molar ratio the PS cylinders were packed in a hexagonal lattice. However, at some lower nonstoichiometric molar ratio, the cylinders packed in a tetragonal lattice. It was discussed that one of the plausible

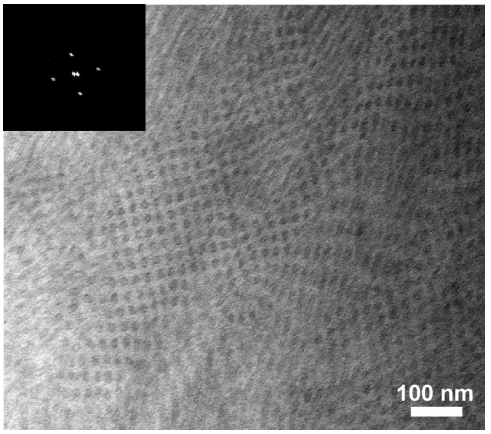

Figure 2. TEM micrograph showing the cross-sectional view of the P4VP(HABA) cylinders in PS-*b*-P4VP(HABA) SMA with $X = 2.0$. The Fourier transform patterns of the real-space images are displayed in the upper left corner. The P4VP(HABA) cylinders are seen to pack in a tetragonal lattice.

reasons for tetragonal lattice was different orientation of the lamellar structure formed by P4VP(DBSA) comb block with respect to the larger length scale structure formed by the copolymer blocks. They further showed that such a packing may result in these systems irrespective of the architecture of block copolymer.[29] However, it is still not clear why tetragonal lattice is stable in such systems at lower nonstoichiometric molar ratios. In the present case, the tetragonal lattice was observed at molar ratio higher than the stoichiometric ratio. Moreover, unlike the system studied by Chen et al.,[28,29] the PS-*b*-P4VP(HABA) system does not form hierarchical structures. Hence, the driving force for the tetragonal lattice in this system should be very different compared to that in the PS-*b*-P4VP(DBSA) system studied by Chen et al. Here, we would also like to note that HABA may tend to aggregate within the P4VP(HABA) cylindrical microdomains because of hydrogen bonding (head-to-head, according to the molecular exciton model) and has been explained well in our previous work.[20,21] Such an aggregation tendency might be much more pronounced at higher molar ratios and could play a role in the tetragonal packing of cylinders observed at $X = 2$. At this stage, we have no solid argument supporting such a hypothesis. However, a detailed study on this issue is beyond the scope of this paper and would require a more intense investigation which we are pursuing at the moment.

Now, we focus on other interesting observation from the SAXS data. The primary scattering peak was observed to shift to low-q region as the molar ratio increased, signaling an increase in the interdomain spacing. The Braggs spacing ($D = 2\pi/q_m$ with q_m being the position of the primary scattering peak) increased from 20 nm for SMA025 to 34 nm for SMA150 as the molar ratio increased (see Supporting Information). The Braggs spacing dropped further to 30 nm for SMA200. It could be noticed that the variation in the Braggs spacing follows the morphological transitions in the SMA. The Braggs spacing showed sudden change after SMA025 since the morphology transformed from bcc packed sphere to hcp packed cylindrical microdomains as the molar ratio increased to SMA050. Again, the sudden drop in the Braggs spacing as molar ratio increased from SMA150 to SMA200 was result of change in morphology from hcp packed cylinders to tetragonally packed cylinders.

The increase in the Braggs spacing and hence the interdomain spacing as the molar ratio increased could be explained in terms of increased chain stretching. Figure 3

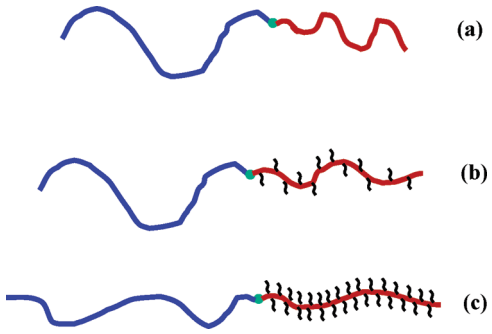

Figure 3. Schematic illustration explaining increased chain stretching at higher HABA/4VP molar ratio (a) neat copolymer, (b) at intermediate HABA/4VP molar ratio, and (c) at high HABA/4VP molar ratio.

shows schematically the effect of increase of molar ratio on block chain conformations in the SMA. As the molar ratio increased, the P4VP chain became more densely grafted with the HABA molecule. Hence, the P4VP chain was expected to had a significantly stretched conformation at higher molar ratio. This not only increased the P4VP(HABA) microdomain size but also led to less interfacial area for PS chains, resulting in its stretching normal to the interface. We must note here that for SMAs with $X < 1$ HABA may not be equally distributed in the P4VP chains. It is possible that because of its aggregation tendency, HABA may tend to pack in a cooperative manner. Such a cooperative packing has been postulated in the past by Chen et al. in the PS-*b*-P4VP(DBSA) SMAs.[28] Furthermore, for $X > 1$, only the model shown in Figure 3 may not explain the increase in interdomain spacing. Here, it is suggested, that the excess HABA distribute homogeneously within the P4VP(HABA) domains, giving a wet-brush-like system known for block copolymer/homopolymer mixtures which additionally contributes to the increased domain spacing.[30]

Microphase Separation in Thin Film. In this section, we will proceed to discuss the microphase separation behavior of SMA in the thin film. First, we will discuss how the solvent affects the microdomain orientation in the SMA, and then the ordering transition in the SMA with respect to annealing time using ex-situ AFM will be presented. All the AFM images discussed in this section were obtained after washing out HABA with methanol. The dark regions in the height images corresponded to holes or empty channels created by the removal of HABA, whereas the light regions corresponded to the PS matrix.

Figure 4 shows the AFM height images of thin films of SMA casted from 1,4-dioxane and further annealed in vapors of 1,4-dioxane. The AFM image of SMA100, SMA075, SMA050, and SMA025 annealed in 1,4-dioxane vapor (Figure 4a−d) showed highly ordered holes packed in a hexagonal lattice on the surface of the film. Such holes could be due to either vertically oriented cylinders or spheres of P4VP(HABA) microdomains. From the composition of the two blocks given in Table 1, cylindrical morphology was expected for SMA100 and SMA075, whereas SMA025 should have spherical morphology. The SAXS results in bulk indeed showed such morphology for these SMAs. However, the composition of SMA050 ($f_{P4VP(HABA)}$ = 17.2) was almost on the border of cylinder and sphere regions in the classical phase diagram of diblock copolymers. In bulk, as discussed above, SAXS revealed hcp cylindrical morphology for SMA050.

In our previous studies on this system, it was shown that, for stoichiometric composition, the SMA annealed in 1,4-dioxane had vertically oriented P4VP(HABA) cylinders in

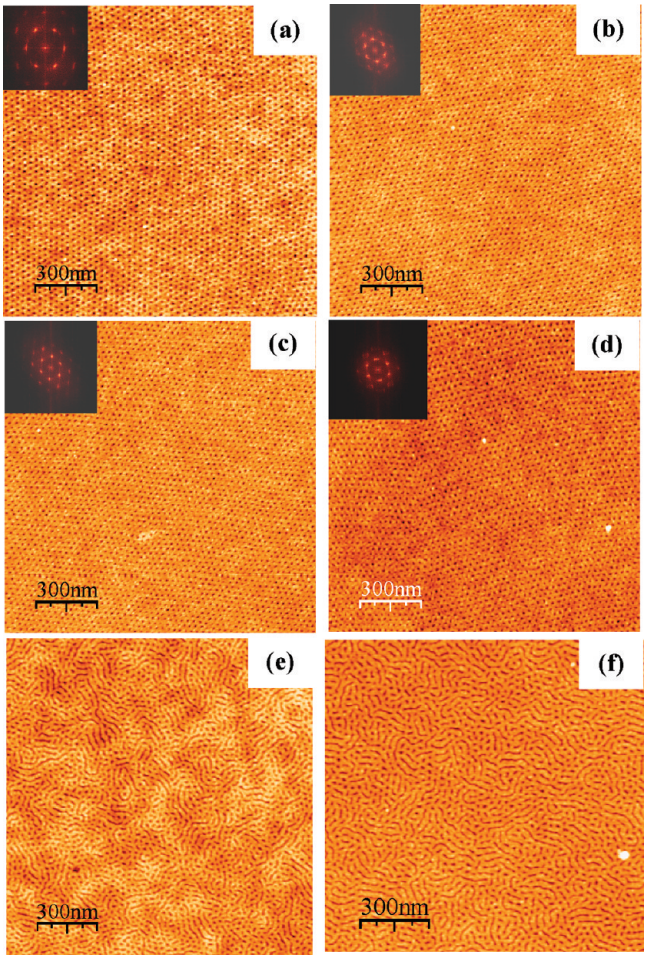

Figure 4. AFM height images obtained for samples casted from 1,4-dioxane solution and then further annealed in 1,4-dioxane vapors: (a) SMA100, (b) SMA075, (c) SMA050, (d) SMA025, (e) SMA150, and (f) SMA200.

PS matrix.[20,21] However, on annealing the SMA in chloroform vapors, P4VP(HABA) cylinders orient parallel to the substrate. We used such a switching phenomenon in this system to determine the morphology of different compositions studied here. The SMA with cylindrical morphology on annealing in chloroform should have cylinders oriented parallel to the substrate, whereas the SMA with spherical morphology will remain unchanged.

Figure 5a−f shows the AFM height images of thin films of SMA casted from 1,4-dioxane solution and then further annealed in chloroform vapors. The figure shows parallel cylindrical structures for SMA100 and SMA075, which were basically empty channels left after washing of HABA (Figure 5a,b), whereas empty holes representing spherical morphology were observed for SMA050 and SMA025 (Figure 5c,d). Hence, the switching of domain orientation was only observed for SMA100 and SMA075. This clearly revealed that as far as morphology in thin films is concerned, SMA100 and SMA075 had P4VP(HABA) cylinders embedded in PS matrix, whereas SMA050 and SMA025 consisted of P4VP(HABA) spheres embedded in PS matrix.

Now, let us focus on the case where SMA contained excess of HABA, i.e., SMA150 and SMA200. The AFM height images show mixed parallel and perpendicular oriented cylinders for SMA150 and SMA200 annealed in 1,4-dioxane vapors (Figure 4e,f). After annealing in chloroform vapors, the morphology still consisted of mixed parallel and

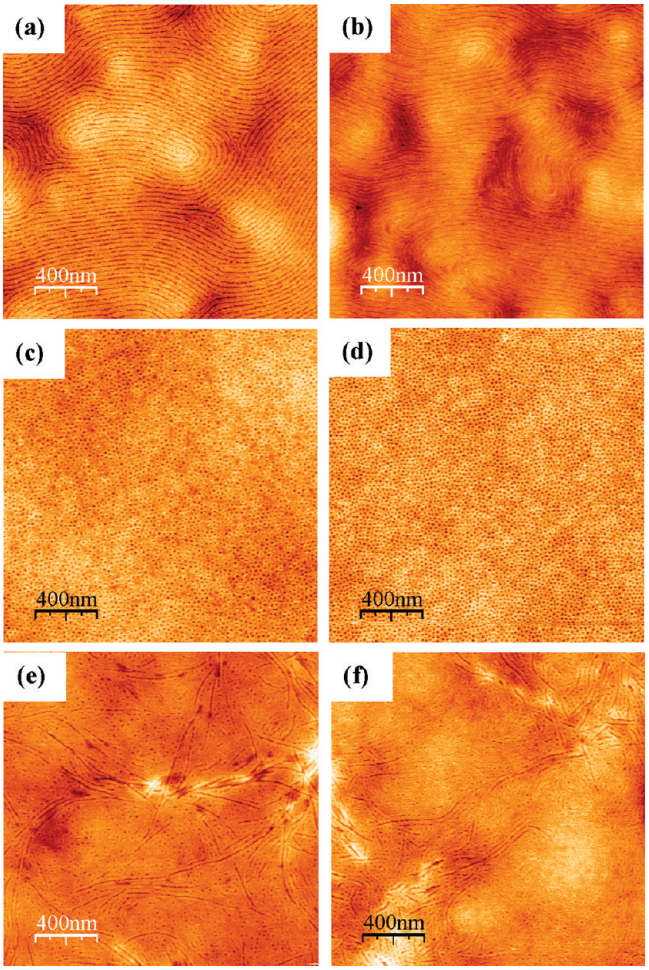

Figure 5. AFM height images obtained for samples casted from 1,4-dioxane solution and then further annealed in chloroform vapors: (a) SMA100, (b) SMA075, (c) SMA050, (d) SMA025, (e) SMA150, and (f) SMA200.

Table 2. Interdomain Spacing at Different HABA/4VP Molar Ratios in Bulk and in Thin Films

system	$d_{1,4\text{-dioxane}}$ [a]	$d_{\text{chloroform}}$ [b]	d_{bulk} [c]
SMA000			25.6
SMA025	29.7	25.1	24.9
SMA050	28.2	26.0	27.8
SMA075	28.4	30.5	30.8
SMA100	29.5	30.0	36.2
SMA150	30.5		38.7
SMA200	31.5		44.4

[a] Interpore distance determined from AFM in thin films annealed in 1,4-dioxane vapors. [b] Interpore distance determined from AFM in thin films annealed in chloroform vapors. [c] Interdomain distance in annealed bulk samples determined from SAXS data. The spacing has been calculated considering bcc packed spherical morphology in SMA000 and SMA025, hcp packed cylindrical morphology in SMA050, SMA075, SMA100, and SMA150, and square packed cylindrical morphology in SMA200.

perpendicular oriented cylinder morphology (Figure 5e,f). However, the laterally oriented cylinders had much larger length than those seen for 1,4-dioxane annealed samples and were randomly distributed on the surface.

Table 2 shows the interdomain spacing obtained from the AFM height images for SMA samples annealed in chloroform and 1,4-dioxane. The interdomain spacing obtained from the SAXS data for bulk samples is also listed in Table 2. It could be observed from the data that the interdomain spacing decreased with decrease in the molar ratio for SMAs having cylindrical morphology, which is consistent with that observed for the bulk samples, as discussed in the previous section. Furthermore, another interesting observation was that for SMA100 and SMA075 the interdomain spacing for samples annealed in chloroform was larger than those annealed in 1,4-dioxane. This has been explained well in the past for SMA100 and is attributed to the distortion of the hexagonal lattice after drying of the film swollen in chloroform vapors.[21] However, the most significant observation noted from Table 2 was the drastic difference in the interdomain spacing of the SMAs in the bulk and that in thin film especially at higher molar ratios. Recently, Ross et al.[31] showed that the domain spacing of a cylinder forming thin films of polystyrene-*block*-poly(dimethylsiloxane) (PS-*b*-PDMS) block copolymer could be tuned with the vapor pressure of a mixed annealing solvent composed of toluene and heptane. It was explained that due to the screening effect of the solvent molecules, the effective Flory−Huggins interaction parameter (χ_{eff}) decreases as the volume fraction (f_s) of solvent in the film increases:

$$\chi_{\text{eff}} = \chi(1 - f_s) \quad (1)$$

where χ is the interaction parameter in the absence of solvent uptake. Consequently, solvent uptake in block copolymer films decreases the effective segregation strength, $\chi_{\text{eff}}N$, where N is the degree of polymerization, and thus affects the equilibrium domain spacing.

In the present case, it was interesting to note that the difference in the domain spacing in 1,4-dioxane annealed thin films and that in bulk samples increased as the HABA fraction increased. This could be explained as follows. 1,4-Dioxane was a selective solvent for PS-*b*-P4VP copolymer, and hence the reduction in the interaction parameter was not expected to be significant when the neat copolymer is exposed to 1,4-dioxane vapors. However, in the case of SMA, the situation will be much more complex. Here, 1,4-dioxane is a good solvent for HABA. Hence, as the molar ratio of the SMA increases, P4VP chains will be covered with more and more HABA molecules. This means that the solubility of P4VP chain in 1,4-dioxane increased at higher molar ratios, or in other words, 1,4-dioxane was a less selective solvent at higher molar ratios. Hence, the interaction parameter will decrease significantly for SMAs with higher molar ratio while they are exposed to 1,4-dioxane vapors and will result in decreased domain spacing than that observed in the bulk.

The increased solubility of P4VP chains at higher molar ratio also explains why mixed morphologies are observed for SMA150 and SMA200 when annealed in 1,4-dioxane vapors. The 1,4-dioxane in this case show similar solubility toward the blocks as that shown by chloroform and is no longer a strongly selective solvent.

Morphological Transition during Orientational Switching of Cylindrical Microdomains in SMA100. In this section, we will discuss about the possible mechanism of the orientational switching observed for cylindrical microdomains of the SMAs when annealed in selective and nonselective solvents. We adopted ex-situ AFM technique for this purpose. SMA100 was investigated as the representative composition for this purpose. Two sets of samples were prepared: one preannealed in 1,4-dioxane vapors, which resulted in hexagonally arranged perpendicular cylinders of P4VP-(HABA), and the other set preannealed in chloroform vapors, which resulted in laterally oriented cylinders of P4VP(HABA). In the next step, samples were annealed in

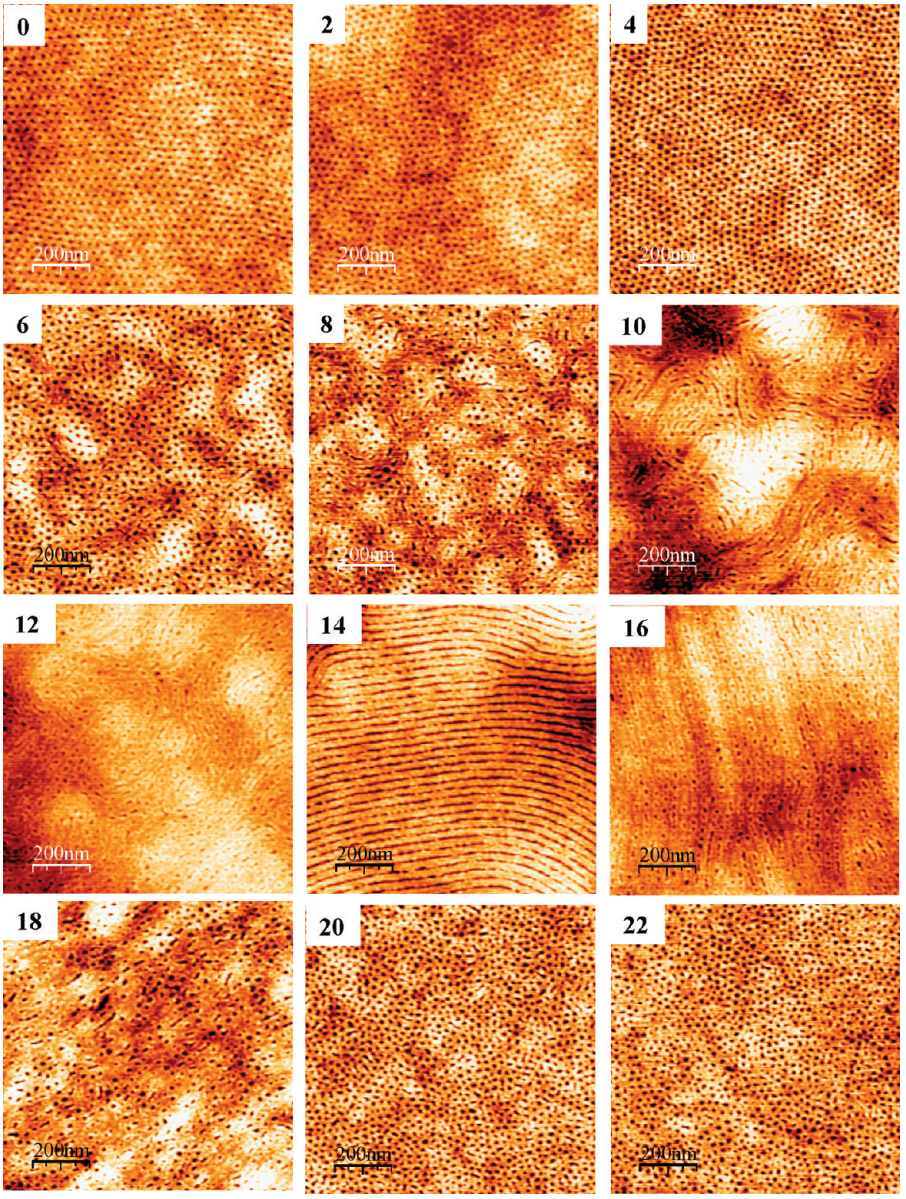

Figure 6. AFM height images of SMA100 samples annealed in 1,4-dioxane vapors and then further annealed in chloroform. The numbers on the AFM images indicates annealing time (in minutes) in chloroform vapors.

the appropriate solvent for different times for switching the domain orientation and, after washing with methanol, were characterized by AFM.

Figure 6 shows the AFM height images of SMA100 samples preannealed in 1,4-dioxane and then further annealed in chloroform vapors for different times. As expected, the preannealed sample show hexagonally packed vertically oriented cylindrical morphology (Figure 6(0)). The morphology remains unperturbed for samples annealed in chloroform for 2 and 4 min. However, noticeable changes in the order and domain shape were observed for sample annealed in chloroform for 6 min. The cylindrical microdomains were not only observed to deform but also observed to connect with the neighboring cylinders. The morphological features for samples annealed for 8 min remained more or less same as the previous one. On further increasing the annealing time, large scale morphological changes were observed. The number of neighboring cylinders coalescing together increased, giving rise to parallel cylindrical microdomains. However, these cylinders were not continuous and consisted of bright regions which as will be discussed below were swollen part of the matrix. The cylinders became more and more continuous as the annealing time was further increased to 14 min. After 16 min of chloroform vapor annealing, well-developed parallel cylindrical morphology was observed in the SMA, indicating complete switching of the domain orientation. Interestingly, on further increasing the annealing time, the cylindrical microdomains were observed to again undergo significant orientational change. The morphological transition was more or less similar to that observed between 6 and 12 min of annealing. Finally, perpendicular oriented cylinders were again observed, however, with poor long-range order. The pathway of orientational switching on annealing in chloroform vapors for SMA075 was same (see Supporting Information).

Similarly, we also studied the switching of in-plane cylinders in SMA100 to perpendicular orientation in 1,4-dioxane vapors (see Supporting Information). On annealing in 1,4-dioxane, the morphological changes observed between 2 and 10 min were essentially the same as that observed during

chloroform annealing in the initial stages. So, instead of very clear empty continuous channels observed in the chloroform preannealed sample, after 1,4-dioxane annealing, though, the cylindrical structure could still be visualized but only with scattered empty pits along its long axis. On further annealing, the large cylinders break into short cylinders and these short cylinders further had pits along the long axis. Interestingly, after annealing for 12 min, the parallel oriented cylindrical microdomains of P4VP(HABA) reappear. These cylindrical structures were not as continuous as those observed for the chloroform preannealed sample. The parallel oriented cylinders further split at the expense of increased density of perpendicularly oriented cylinders on increasing the annealing time. The perpendicularly oriented cylinders were observed to locate in the regions previously occupied by parallel cylinders. Finally, on annealing for 20 min, only perpendicular cylinders are observed in the SMA film. It was interesting to note here that switching from parallel to perpendicular orientation took much longer time than vice versa. This could be attributed to the low vapor pressure of 1,4-dioxane compared to chloroform at the room temperature annealing condition.

Discussion on Domain Orientation Switching. We now discuss the possible mechanism and the transient pathways involved during switching of the orientation of cylindrical microdomains based on the AFM results discussed above. The silicon substrate is known to be attractive for P4VP block, and hence, the substrate−film interface will be enriched in P4VP chains.[32,33] Moreover, since PS has lower surface energy, it is expected to occupy the film−air interface. It is well-known that the microdomain orientation in case of thin film casted on substrate having preferential attraction for one block is in-plane. However, factors like film thickness, solvent evaporation rate, and the selectivity of the solvent may further influence the domain orientation.[34−36] In the present case, chloroform was nonselective solvent whereas 1,4-dioxane was a selective solvent for PS block. Furthermore, whereas HABA has excellent solubility in 1,4-dioxane, its solubility in chloroform is limited (0.6% maximum). Hence, the selectivity of the two solvents was expected to be different for the PS-*b*-P4VP(HABA) SMA than that for the pure PS-*b*-P4VP diblock.

The switching of the microdomain orientation from in-plane to vertical morphology has been studied in the past by Russell et al.[37] The switching was induced by the application of electric field. It was found that the mechanism in such a case involved several steps of morphological changes while the electric field is being applied. The applied electric field enhanced the fluctuations at the interfaces of the cylindrical microdomains aligned parallel to the surface. The growth of fluctuations continued until the cylindrical microdomains broke up into spherical microdomains. The spherical microdomains then deformed into ellipsoidal domains that reconnected into cylindrical microdomains oriented at 45° with respect to the applied field direction. Further annealing aligned the tilted cylinders along the applied field direction.

The switching of domain orientation in the present case was much more complex and involved solvent as the driving force. Swelling in solvent vapor will result in changes in the volume fraction of the two phases and will also affect the effective interaction parameter between the two blocks. Figure 7 shows the phase diagram of block copolymers in the composition range of interest for the present investigation. As stated previously, the actual phase diagram of the SMA might be slightly different than that shown in Figure 7. Nevertheless, we did not expected this to had a significant

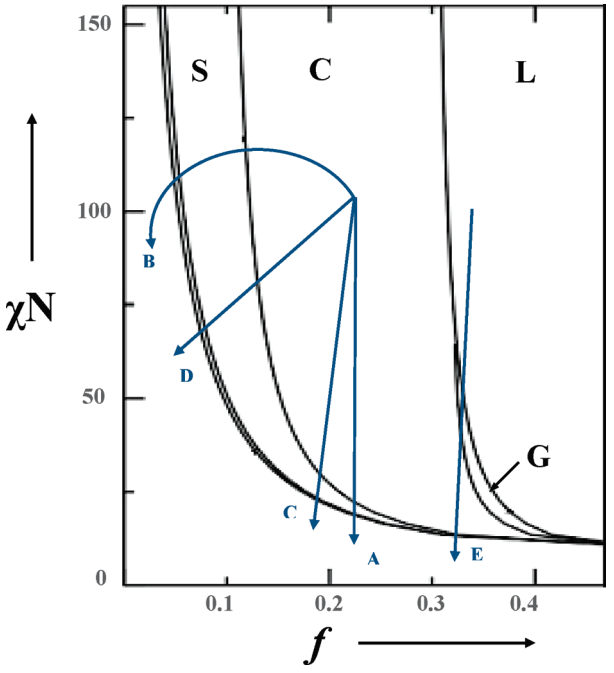

Figure 7. Schematic phase diagram showing the effect of swelling on SMA100 in different solvents. Trajectory A represents swelling in a nonselective solvent, B represents swelling in strongly PS selective solvent, C represents swelling in chloroform vapors, and D represents swelling in 1,4-dioxane vapors. Trajectory E represents swelling of SMA200 in chloroform vapors.

effect on the following discussions. Green and co-workers[38] recently have explained the effect of solvent swelling on the phase behavior of block copolymers. According to them, when an AB diblock is exposed to solvent, the effective interaction parameter (χ_{eff}) will change to

$$\chi_{eff} \sim \varphi(\chi_{AB} + \Delta\chi) = \varphi(\chi_{AB} + \chi_{A-S} - \chi_{B-S}) \qquad (2)$$

where φ is the volume concentration of copolymer in the solvent and $\Delta\chi$ is the difference between the A-solvent and B-solvent interaction parameters χ_{A-S} and χ_{B-S}. Here, it is assumed that χ_{A-S} and χ_{B-S} are not strongly concentration dependent. In the case of a neutral solvent, $\Delta\chi \sim 0$. Thus, when a neutral solvent is added to a block copolymer system, the decrease in φ effectively decreases $\chi_{eff}N$, with N being the total copolymer length. The system, hence, will go toward disordered state. This corresponds to the vertical trajectory A shown in the phase diagram in Figure 7. Here, the origin point of the trajectory is placed at a position corresponding to SMA100 composition. In the case of strongly selective solvent, since $\Delta\chi > 1$, decrease in φ may result in increase in χ_{eff} for low swelling ratios when $\Delta\chi$ dominates. For high enough swelling φ will dominate, resulting in a decrease of χ_{eff} again. Moreover, the selective solvent will exclusively go to one of the blocks, increasing the volume fraction of this block. Hence, swelling in a strongly selective solvent may essentially lead to a curved trajectory B in the phase diagram as shown in Figure 7. In the present case, chloroform is a nonselective solvent for PS and P4VP block. However, since the solubility of HABA in chloroform is limited, the solvent will be more preferential for the PS block (see Supporting Information). Hence, the SMA100 in chloroform will most likely to follow the trajectory C shown in Figure 7. Similarly, 1,4-dioxane is a selective solvent for PS block but at the same time is a good solvent for HABA and thereby will decrease the selectivity of the solvent for PS block in the SMA (see

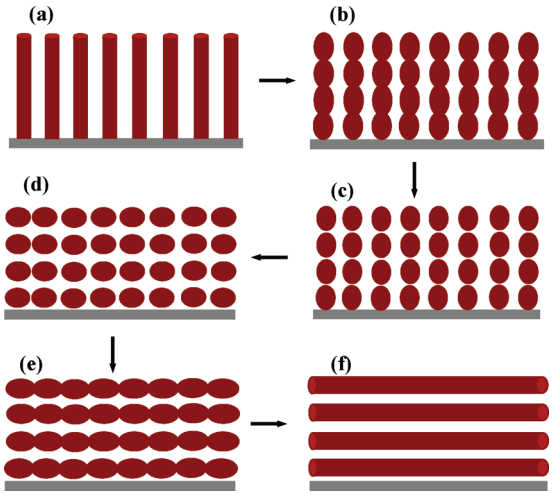

Figure 8. Schematic illustration explaining pathways involved in switching of the perpendicular orientation of P4VP(HABA) cylinders to parallel in chloroform vapors (a) side view of perpendicular oriented cylinders; (b) undulation of the interface; (c) breakup of cylinders into ellipsoid; (d) switching of the long-axis of ellipsoids parallel to the surface; (e) coalescence of the ellipsoids along the surface plane producing parallel cylinders (f).

Supporting Information). Hence, the SMA100 in 1,4-dioxane will follow trajectory D shown in Figure 7.

Now, we consider the case of switching from perpendicular cylinder to parallel cylinders in chloroform vapors. As the SMA film is swelled in chloroform vapors, the solvent goes to both PS and P4VP(HABA) phases and increases the mobility of the chains. Since perpendicular cylinders are metastable structures, they will preferably try to align parallel to the substrate under favorable conditions. Hence, once enough motion is imparted to the polymer chains by the chloroform vapors, interface fluctuations in the perpendicular cylinders are induced, driven by the thermodynamic instability of the perpendicular interface. This will bring about undulation in the cylindrical domains similar to that reported for transformation of HCP cylinders to bcc packed spheres,[39] as shown schematically in Figure 8b. The undulated cylinders then break into ellipsoids (Figure 8c) and start coalescing with the ellipsoids formed from the neighboring cylinder along the plane of the substrate (Figure 8d,e). The AFM images prove such a coalescence mechanism. As could be observed in Figure 6, the AFM images obtained between 8 and 12 min of chloroform annealing shows pits (dark areas) with swollen part (bright areas) in-between. Such a morphology was expected if the system were in stage d or e shown in Figure 8. Here, during washing with methanol, HABA will preferably try to escape from the region close to the surface which are seen as pits. At the same time, the coalescing portion of the two nearby ellipsoid domains will just swell together with the overlaying PS matrix because of methanol absorption by the P4VP(HABA) blocks. Such a coalescence process ultimately leads to the formation of fully developed parallel oriented cylindrical microdomains of P4VP(HABA) blocks (Figure 8f). It must be noted that while all this domain realignment is taking place, the SMA is still very much in the cylindrical region of the phase diagram. However, at high enough swelling, the SMA goes into the spherical region of the phase diagram as could be seen from the trajectory D in Figure 7. At this moment, because of the interfacial fluctuations, the cylindrical domains again break into ellipsoidal microdomains which then attain a spherical morphology which should be packed in a bcc lattice. Now, this bcc packed spherical morphology of SMA is in swollen state. Hence, as soon as the sample is taken out from the chamber, the solvent evaporates quickly and the spherical microdomains of P4VP(HABA) merge along the thickness of the film, resulting in standing P4VP(HABA) cylinders again. Ideally, at high enough swelling, the SMA should go into a disordered state. However, during our studies we never reached such a state since the film started to dewet. It must be noted here that the height and number of layers of cylinder as shown in Figure 8 are just for the illustration of the plausible pathway and do not exactly correspond to those actually in the thin films used in the experiments. The film thickness in the present case is 40 nm, and a domain periodicity of 20−30 nm will mean 2−3 layers of in-plane cylinders depending on the thickness of terraces. In the case of perpendicular cylinders, since the cylinder diameter is ~8 nm, the aspect ratio of the cylinder should be more than 4.

For the case of switching from parallel to perpendicular orientation in 1,4-dioxane vapors the mechanism was very much similar to that explained above for the case of reorientation of parallel cylinders to perpendicular at high enough swelling in chloroform vapors. So, in this case, as the SMA is swelled in 1,4-dioxane vapors, the sample follows the path D in Figure 7. Solvent goes selectively to PS phase, and hence, the system goes into bcc packed spherical morphology via domain breakup of cylinders. These spheres then merge along the thickness of the film to produce the perpendicular cylinders as explained in our previous work.[21]

Morphological Transition during Solvent Vapor Annealing in SMA200. In the end, we shortly report on the case of morphology realignment during swelling of SMA200 which had an excess of HABA. Figure 9 shows the ex-situ AFM images obtained for this sample after swelling in chloroform for different times. According to the phase diagram shown in Figure 7, the SMA with this composition was expected to have a lamellar morphology. However, at the same time, the position was close to cylindrical and gyroid region in the phase diagram. The as-casted sample showed morphological features which gave an impression of a distorted cocontinuous morphology. However, when the sample was swelled in chloroform for a short time and after drying washed with methanol to remove HABA, the AFM image interestingly showed hexagonally packed PS dots on the surface. The origin of such morphology could be understood by looking into the phase diagram shown in Figure 7. On the basis of solvent selectivity, the SMA200 is expected to follow a trajectory E while being swelled in chloroform. Hence, for small swelling ratios, the sample will go to the gyroid region in the phase diagram. It has been reported that such morphology is difficult to be achieved in a thin film like being used in this work, and these conditions may lead to the generation of hexagonally perforated layer which is a metastable structure and has been widely observed around this region of the phase diagram.[40,41] The hexagonally perforated morphology consists of alternating layers of the two components with hexagonally packed cylindrical perforations of the majority component in the layer formed by the minority component. The AFM images obtained after 3 and 5 min of chloroform annealing clearly show this morphology (Figure 9). The top layer consisted of P4VP(HABA) blocks with perforations of PS, and on washing with methanol, HABA goes out, leaving P4VP chains collapsed on the wall of P4VP cylinders. This shows that pathway-dependent self-assembly in block copolymer thin films may lead to some interesting nonequilibrium morphologies which is drastically different from its equilibrium morphology. It must be mentioned here that the hexagonally perforated layer

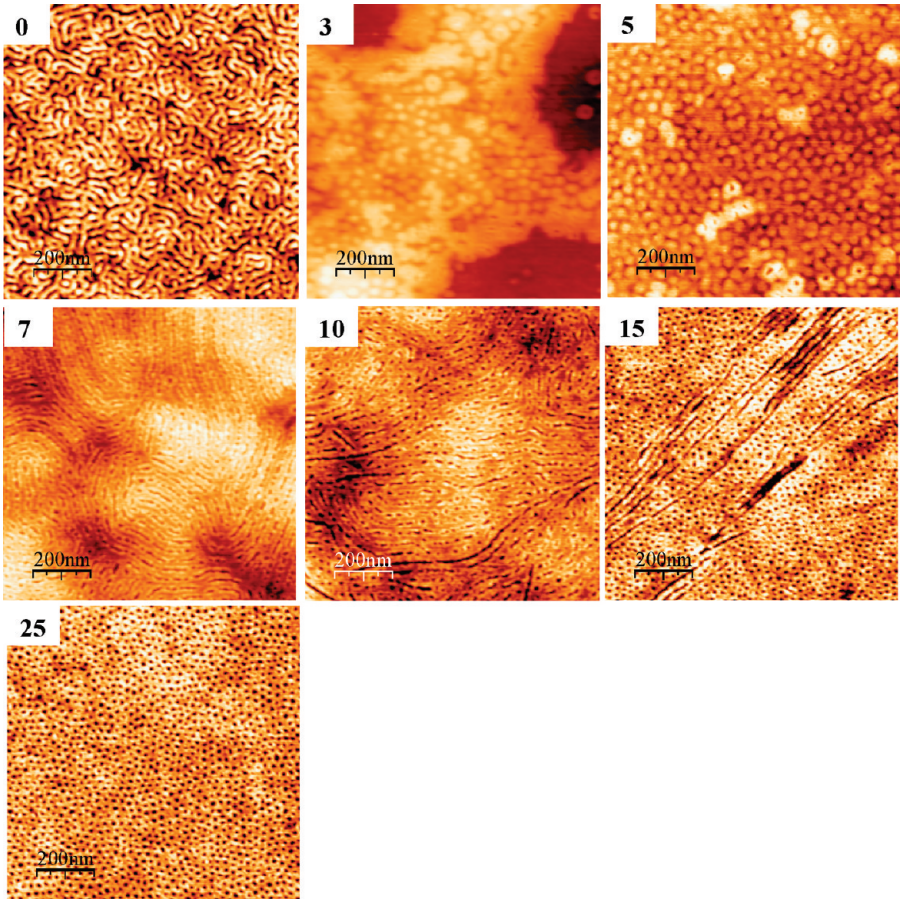

Figure 9. AFM height images of SMA200 samples casted from 1,4-dioxane solution and then further annealed in chloroform. The numbers on the AFM images indicate annealing time (in minutes) in chloroform vapors.

morphology was also observed for SMA150 under similar conditions (see Supporting Information).On further swelling, the SMA200 goes into the cylindrical region of the phase diagram, and since chloroform is a nonselective solvent, the cylindrical microdomains observed were mostly aligned parallel to the substrate. However, as in the previous cases, at higher swelling, the system may move into the spherical region of the phase diagram, and this scenario produced perpendicular cylinders by the mechanism discussed above and was clearly observed in the AFM images.

Conclusions

The SMA's formed by PS-*b*-P4VP with HABA were investigated in a range of molar ratio (X = HABA/4VP ratio) both in bulk and in thin films. In bulk, the SMA showed spherical morphology with P4VP(HABA) spheres packed in a bcc lattice in PS matrix when $X < 0.5$. For $0.5 \leq X < 2.0$, the SMA showed cylindrical microdomains of P4VP(HABA) packed in a hexagonal lattice in PS matrix. However, interestingly, the SMA composition corresponding to $X = 2.0$ showed square-packed cylinders of P4VP(HABA) block, the origin of which is still not clear. In thin film, the SMA with $X \leq 0.5$ showed spherical microdomains of P4VP(HABA) block, whereas at higher molar ratio the morphology was cylindrical. The orientation of cylindrical microdomains of P4VP(HABA) depended on the selectivity of the solvent as well as on the degree of swelling. Hence, in a nonselective solvent like chloroform the cylinders were found to lie parallel to the substrate as long as the swelling ratio allowed the system to be in the cylindrical region of the phase diagram. At high swelling ratio the cylinders transforms into spherical domains, and drying of the solvent resulted in perpendicular orientation. In a selective solvent like 1,4-dioxane, the cylinders were found to be always oriented perpendicular to the substrate for $0.5 < X < 1.5$. Such a morphology was favored in this case, since even at a small degree of swelling, the system went into spherical morphology which ultimately resulted in perpendicular cylinders. The transformation from perpendicular to parallel domain orientation in chloroform involved domain breakup, induced by thermodynamically unstable interface, and then coalescence of the domains along the plane of the film. Moreover, at excess HABA concentration, a hexagonally perforated lamellar morphology was observed when the system was shortly exposed to chloroform.

Acknowledgment. The authors thank Dr. Peter Formanek and Mr. Andriy Horechyy for their help in the TEM measurements. This research was supported by the priority program of Deutsche Forschungsgemeinschaft (SPP1165, Project No. STA324/31-2).

Supporting Information Available: SAXS profile of SMA200; temperature-dependent SAXS profiles of neat HABA; plot depicting variation of Braggs spacing with HABA/4VP molar ratio; AFM images of as-casted SMA samples; AFM images of SMA075 and SMA150 annealed in chloroform for different times; AFM images of SMA100 annealed in 1,4-dioxane for different times; plot depicting relative swelling of P4VP+HABA and PS thin films in 1,4-dioxane and chloroform.This material is available free of charge via the Internet at http://pubs.acs.org.

References and Notes

(1) Whitesides, G. M.; Grzybowski, B. *Science* **2002**, *295*, 2418–2421.
(2) Hamley, I. W. *Angew. Chem., Int. Ed.* **2003**, *42*, 1692–1712.

(3) Darling, S. B. *Prog. Polym. Sci.* **2007**, *32*, 1152–1204.
(4) Segalman, R. A. *Mater. Sci. Eng., R* **2005**, *48*, 191–226.
(5) Krishnamoorthy, S.; Hinderling, C.; Heinzelmann, H. *Mater. Today* **2006**, *9*, 40–47.
(6) Olson, D. A.; Chen, L.; Hillmyer, M. A. *Chem. Mater.* **2008**, *20*, 869–890.
(7) Ruzette, A.-V.; Leibler, L. *Nat. Mater.* **2005**, *4*, 19–31.
(8) Bates, F. S.; Fredrickson, G. H. *Phys. Today* **1999**, *52*, 32–38.
(9) Krausch, G.; Magerle, R. *Adv. Mater.* **2002**, *14*, 1579–1583.
(10) Ikkala, O.; ten Brinke, G. *Science* **2002**, *295*, 2407–2409.
(11) Ikkala, O.; ten Brinke, G. *Chem. Commun.* **2004**, 2131–2137.
(12) Mäkinen, R.; de Moel, K.; de Odorico, W.; Ruokolainen, J.; Stamm, M.; ten Brinke, G.; Ikkala, O. *Adv. Mater.* **2001**, *13*, 107–121.
(13) Nandan, B.; Gowd, E. B.; Bigall, N.; Eychmüller, A.; Formanek, P.; Simon, P.; Stamm, M. *Adv. Funct. Mater.* **2009**, *19*, 2805–2811.
(14) Albrecht, K.; Mourran, A.; Zhu, X.; Markkula, T.; Groll, J.; Beginn, U.; de Jeu, W. H.; Moeller, M. *Macromolecules* **2008**, *41*, 1728–1738.
(15) van Zoelen, W.; Asumaa, T.; Ruokolainen, J.; Ikkala, O.; ten Brinke, G. *Macromolecules* **2008**, *41*, 3199–3208.
(16) van Zoelen, W.; Polushkin, E.; ten Brinke, G. *Macromolecules* **2008**, *41*, 8807–8814.
(17) Tung, S.-H.; Kalarickal, N. C.; Mays, J. W.; Xu, T. *Macromolecules* **2008**, *41*, 6453–6462.
(18) Tung, S.-H.; Xu, T. *Macromolecules* **2009**, *42*, 5761–5765.
(19) Tokarev, I. PhD Dissertation, Technische Universität Dresden, **2005**.
(20) Sidorenko, A.; Tokarev, I.; Minko, S.; Stamm, M. *J. Am. Chem. Soc.* **2003**, *125*, 12211–12216.
(21) Tokarev, I.; Krenek, R.; Brukov, Y.; Schmeisser, D.; Sidorenko, A.; Minko, S.; Stamm, M. *Macromolecules* **2005**, *38*, 507–516.
(22) Zschech, D.; Milenin, A. P.; Scholz, R.; Hillebrand, R.; Sun, Y.; Uhlmann, P.; Stamm, M.; Steinhart, M.; Gosel, U. *Macromolecules* **2007**, *40*, 7752–7754.
(23) Seifarth, O.; Krenek, R.; Tokarev, I.; Burkov, Y.; Sidorenko, A.; Minko, S.; Stamm, M.; Schmeisser, D. *Thin Solid Films* **2007**, *515*, 6552–6556.
(24) Luchnikov, V.; Kondyurin, A.; Formanek, P.; Lichte, H.; Stamm, M. *Nano Lett.* **2007**, *7*, 3628–3632.
(25) Martn-Rapn, R.; Marcos, M.; Omenat, A.; Barber, J.; Romero, P.; Serrano, J. L. *J. Am. Chem. Soc.* **2005**, *127*, 7397–7403.
(26) Mogi, Y.; Nomura, M.; Kotsuji, H.; Ohnishi, K.; Matsushita, Y.; Noda, I. *Macromolecules* **1994**, *27*, 6755–6760.
(27) Tang, C.; Lennon, E. M.; Fredrickson, G. H.; Kramer, E. J.; Hawker, C. J. *Science* **2008**, *322*, 429–432.
(28) Chen, H. L.; Lu, J. S.; Yu, C. H.; Yeh, C. L.; Jeng, U. S.; Chen, W. C. *Macromolecules* **2007**, *40*, 3271–3276.
(29) Chiang, W.-S.; Lin, C.-H.; Yeh, C.-L.; Nandan, B.; Hsu, P.-N.; Lin, C.-W.; Chen, H.-L.; Chen, W.-C. *Macromolecules* **2009**, *42*, 2304–2308.
(30) Tanaka, H.; Hasegawa, H.; Hashimoto, T. *Macromolecules* **1991**, *24*, 240–251.
(31) Jung, Y.-S.; Ross, R. A. *Adv. Mater.* **2009**, *24*, 2540–2545.
(32) Liu, Y.; Zhao, W.; Zheng, X.; King, A.; Singh, A.; Rafailovich, M. H.; Sokolov, J.; Dai, K. H.; Kramer, E. J.; Schwarz, S. A.; Gebizlioglu, O.; Sinha, S. K. *Macromolecules* **1994**, *27*, 4000–4010.
(33) Yokoyama, H.; Mates, T. E.; Kramer, E. J. *Macromolecules* **2000**, *33*, 1888–1898.
(34) Kim, G.; Libera, M. *Macromolecules* **1998**, *31*, 2569–2577.
(35) Kim, S. H.; Misner, M. J.; Xu, T.; Kimura, M.; Russell, T. P. *Adv. Mater.* **2004**, *16*, 226–231.
(36) Ho, R.-M.; Tseng, W.-H.; Fan, H.-W.; Chiang, Y.-W.; Lin, C.-C.; Ko, B.-T.; Huang, B.-H. *Polymer* **2005**, *46*, 9362–9377.
(37) Xu, T.; Zvelindovsky, A. V.; Sevink, G. J. A.; Lyakhova, K. S.; Jinnai, H.; Russell, T. P. *Macromolecules* **2005**, *38*, 10788–10798.
(38) Li, Y.; Wang, X.; Sanchez, I. C.; Johnston, K. P.; Green, P. F. *J. Phys. Chem. B* **2007**, *111*, 16–25.
(39) Kimishima, K.; Koga, T.; Hashimoto, T. *Macromolecules* **2000**, *33*, 968–977.
(40) Knoll, A.; Magerle, R.; Krausch, G. *J. Chem. Phys.* **2004**, *120*, 1105–1116.
(41) Park, I.; Park, S.; Park, H.-W.; Chang, T. *Macromolecules* **2006**, *39*, 315–318.